Characterization of NPP Visible/Infrared Imager Radiometer Suite (VIIRS) reflective solar bands dual gain anomaly

Shihyan Lee, Jeff McIntire, Hassan Oudrari

Sigma Space Corporation, Lanham, MD, 20706, USA

Submitted to SPIE

xxx, 2012

ABSTRACT

The Visible/Infrared Imager Radiometer Suite (VIIRS) contains six dual gain bands in the reflective solar spectrum. The dual gain bands are designed to switch gain mode at pre-defined thresholds to achieve high resolution at low radiances while maintaining the required dynamic range for science. During pre-launch testing, an anomaly in the electronic response before transitioning from high to low gain was discovered and characterized. On-orbit, the anomaly was confirmed using MODIS data collected during Simultaneous Nadir Overpasses (SNOs). The analysis of the Earth scene data shows that dual gain anomaly can be determined at the orbital basis. To characterize the dual gain anomaly, the anomaly region and electronic offsets were tracked per week during the first 8 month of VIIRS operation. The temporal analysis shows the anomaly region can drift ~20 DN and is impacted by detectors' DC Restore. The estimated anomaly flagging regions cover ~2.5 % of the high gain dynamic range and are consistent with prelaunch and on-orbit LUT. The prelaunch results had a smaller anomaly range (30 – 50 DN) and are likely the results of more stable electronics from the shorter data collection time. Finally, this study suggests future calibration efforts to focus on the anomaly's impact on science products and possible correction method to reduce uncertainties.

Keywords: NPP, VIIRS, dual gain band, anomaly, reflective solar bands

1. Introduction

The dual gain radiometric band is one of the unique design features of the Visible Infrared Imaging Radiometer Suite (VIIRS) from its heritage instruments. The dual gain capability allows signal detection over a wide range of photon flux conditions. At each observation, the gain state is transmitted through a separate gain output to determine the gain specific calibration coefficients. Compare to heritage instruments' two bands design [1], the single dual gain band assured geometric and radiometric identity between the low and high gain band. Combining low and high gain bands into a single dual gain band also reduce the physical space requirement on the focal plane.

The VIIRS on board of the NPP satellite consist 6 dual gain bands within Visible Near-InfraRed (VisNIR) spectrum. In April 2006, a Dual Gain Anomaly (DGA) for VisNIR dual gain bands was observed during VIIRS Engineering Design Unit (EDU) sensor-level testing. In July 2007, the attempt to fix the DGA on Fight Unit 1 (FU1) was found to be unsuccessful. The subsequent analyses concluded the best option was to characterize the VIIRS DGA and implement a flagging algorithm into SDR software package [2, 3]. Observations show the VIIRS F1 DGA usually happens around the 90% of the gain switching point. One possible root cause of the DGA has been identified as the non-linear response in the Read Out Integrated Circuit (ROIC) during the short time period when the comparator is active (around 90% of gain switching point) [2]. Since the comparator compares the received voltage with some pre-defined threshold to determine the read out gain mode, the anomaly is driven by read out voltage. For the same input radiance, the read out voltage could be slightly different depending on the detector's gain and DC Restore (DCR). Fortunately, only a small portion of the dynamic range is affected as the signal-to-response becomes linear again after the comparator finishes the query.

This paper will characterize VIIRS DGA on-orbit features and compare them with the results derived from pre-launch test data. An automatic method will be presented to determine DGA flagging region and the anomaly regions will be tracked in multiple time periods to characterize on-orbit temporal variability. Finally, the determined DGA range will be compared with pre-launch [4, 5] and official on-orbit DGA LUT updates [6].

2. Dual Gain Anomaly Characteristics

During pre-launch testing, the dual gain anomaly was best characterized using measurements from Radiometric Characterization Test II (RC-2) [4, 5]. In RC-2, VIIRS scans through the Spherical Integrated Source (SIS-100). During a scan, the anomaly can be observed from the partial views of the SIS aperture where the target radiance gradually increased or decreased (Figure 1). In the Figure, DGA regions are highlighted and were determined by the abnormal increase followed by a decrease in DN ramp slope and noise [5, 6]. The RC-2 test offers many radiance levels [7], which ensured that the DGA was observed multiple times in different spectral resolution allowing cross validating and a more precise characterization [5].

However, the ramp up/down method is not suitable for determining the DGA on-orbit as a similar real world target does not exist. Fortunately, the radiance distributions near expected anomaly regions are favorable for another pre-launch DGA tracking method [2, 3]. This method determines DGA regions based on the expected histogram signature produced by the anomaly from randomly distributed input radiances.

Figure 2 shows the DN histogram for the band M1 detector 1 using the same data as in Figure 1. The nonlinear increase and decrease in DGA DN ramp feature (Figure 1) implies a DN histogram having decreasing counts in lower part of anomaly region and sharply increasing counts when approaching upper limits of the anomaly. Such features are observed in Figure 2 in the same anomaly region shown in Figure 1. However, determining DGA range in Figure 2 is

not straight forward as the histogram generated from the limited tested SIS-100 radiance levels could have false peaks/valleys. The false peaks and valleys are caused by the input radiance distribution but not the true DGA. To best quantify DGA region within its histogram feature, the randomly distributed input radiance is desired to reduce anomaly determination uncertainties.

To confirm the DGA persisted after launch, and the on-orbit observation can be used to characterize the anomaly by its histogram features, the MODIS data collected during Simultaneous Nadir Overpasses (SNOs) with VIIRS were analyzed. Figure 3 shows histograms of MODIS bands with similar bandpass to VIIRS VisNIR dual gain bands. In the plots, the red boxes indicate regions near the DGA as defined pre-launch. The MODIS histograms within the red boxes are nearly flat, indicating near random distributions ideal for observing the DGA.

Figure 4 shows the histograms of the matching VIIRS VisNIR dual gain bands (detector 8 shown). The VIIRS histograms are nearly flat except for areas affected by the DGA. Note, the slight differences between MODIS (Figure 3) and VIIRS (Figure 4) histograms are expected due to the small difference in SNO timing/location, bandpass and spatial resolutions. Figure 5 shows the VIIRS DN histograms from a recently collected orbit (3000). All VisNIR dual gain bands show similar features as in Figure 4 including bands M5 and M7, which do not correlate exactly to any MODIS bands.

3. Tracking Dual Gain Anomaly on-orbit

The DGA needs to be determined at each detector for all VisNIR dual gain bands. A robust and efficient method is needed to determine the DGA anomaly in a timely fashion to monitor the DGA regions over time for potential drift [8, 9].

3.1 Use complete orbit earth scene data

To simplify data collection, a full-orbit of Earth scene data was used to generate the histogram for DGA analysis. The DN histograms in Figure 5 show a well defined histogram feature for characterizing DGA. The near random distribution is primarily because the DGA regions are not near prominent surface types, i.e. ice or ocean. The moderate VIIRS spatial resolution (750 m at nadir) implies a high percentage of mixed pixels could fall near DGA regions, i.e. edge of cloud over the ocean or mixed land cover types. Other factors like Earth scene variation in sun – view angle geometry, atmospheric condition etc., also results in a more randomly varied DN distribution when the sample region is large enough. Therefore, the use of DN histograms from one complete orbit of Earth scene data is to increase both the data randomness near the DGA region and statistical significance. As shown in Figure 5, the DN histograms for the dual gain bands (detector 8) have minimum of 800 counts for each bin (DN value) near the DGA region. Such statistical significance should ensure robust operational DGA determinations.

Table 1 lists the orbits analyzed in this analysis which covers more than 8 months after the VIIRS opened its nadir door on 11/21/2011. The data was selected where the DC Restore (DCR) offset

were constant throughout the orbit. A changing DCR offset will blur DGA boundary as the anomaly regions could shift depending on DCR offset [2, 3].

3.2 Determine DGA boundary in histogram

The DN ranges affected by the anomaly were determined by the expected DGA histogram features based on observed input-vs.-response curves (Figures 1 and 2). The DGA boundaries are determined based on the following steps:

1. The histogram curve is smoothed to reduce small variations in the DN distribution. Figure 6 shows an example of a histogram curve before (top) and after smoothing (bottom).
2. Identify the lower and upper peak. These peaks are well defined features within the anomaly region, and are used as the initial reference points when determining the anomaly boundary.
3. Starting from the above determined references points and stepping forward in DN, find the closest DN value where the first derivative (slope) becomes smaller than the expected histogram slope. The expected histogram slope is determined using points outside the anomaly region. In Figure 6, the blue and red vertical lines indicate the lower and upper bound of the anomaly.

The above method determines the DGA boundary by the most prominent histogram features so that all detectors can be tracked with low uncertainties. However, this method determines DGA boundary more conservatively for the upper bound and less conservatively for the lower bound. This is based on the cross examination of the DN histogram results with the DN ramp from pre-launch data. The possibility of slightly over/under estimated anomaly range is a limitation of this histogram method. However, the DGA boundary can be more consistently determined using randomly selected orbital Earth scene data to track the DGA temporal variations.

4. Results

Based on the method described above, the DGA range was determined roughly every 100 orbits (7 days) with additional orbits analyzed during intensive Calibration/Validation (Cal/Val) period (year 2011) (see Table 1). The results are then compared with pre-launch values and the updated on-orbit DGA LUT [6].

4.1 Temporal Characteristics

The time series of DGA boundaries for each analyzed orbit are plotted in Figure 7. The temporal trend of the anomaly's upper and lower boundaries shows small increases from orbit 360 to 440 followed by small decreases afterward. One possible reason for such a drift could come from the VisNIR focal plane and electronic temperature drift [11]. The pre-launch testing had shown the DGA can drift up to 50 DN from the cold to hot temperature plateau [4, 5]. Additionally, the lower and upper boundary seems to drift at similar rate, keeping the anomaly affected DN range roughly the same over time.

Figure 7 shows the DGA boundary drift is ~20 DN within the analyzed orbits, which cover over 8 months after VIIRS opens its nadir door to collect Earth scene data. In the same period, VIIRS had experienced major events like 1394 anomalies, pitch/yaw maneuvers, opening of Cryo-Cooler door, OBC warm-up/cool-downs and stowed the RTA telescope multiple times (Table 2). The results indicate these VIIRS and/or spacecraft events likely have minimal influence on DGA characteristics.

4.2 DC Restore

Although the data is selected with no DCR variation within the orbit, the DCR offset could still be different from one orbit to another. In addition, the DCR is Half Angle Mirror (HAM) side dependent, but the DGA range is not, which results in additional DCR difference.

In Figure 8, the DC Restore offset variation (Delta DCR) for the analyzed orbits are calculated as the difference between the orbital DCR offset and the first analyzed orbit (360). Figure 8 shows the Delta DCR drifts are within ~15 DN and the drift patterns are similar for all dual gain bands. The previous studies [2 – 5] showed the DCR offset change is one of the primary driving forces in DGA boundary shift as the anomaly is found to be determined by the combine detector and DCR inputs to the instrument's electronics. The drift in Delta DCR should indicate a similar change in DGA range. Comparing Figure 7 and 8, the DGA drift shows temporal trends that are correlated to Delta DCR change for the corresponding bands.

The small DCR variation is normal as the VIIRS DCR algorithm is designed to maintain the dark offset to within a small pre-defined target range [10]. The electronic dark current could also change slightly depending on the instrument condition, i.e. temperature. Therefore, a buffer should be added to DGA range determined from a certain orbit to include potential anomaly drift. Such a buffer might be estimated from the relationship of the dark offset, targets, instrument conditions and the expected DCR behavior if they are well characterized [2, 3].

4.3 DGA flagging LUT

To generate the VIIRS SDR DGA flagging LUT, the bounds of the anomaly range found in all analyzed orbits are used. As each orbit has slightly different DCR and orbital dark offsets, the outer bounds of all DGA ranges will include the anomaly range in many different operational conditions. Therefore, the extended anomaly range encompass DGA from multiple orbits could approximate the per-orbit DGA with the extended buffer to flag the anomaly under different DCR, dark offset and instrument conditions. This DGA flagging LUT is expected to be a slightly over-flagging as the instantaneous DGA range is expected to be somewhere within the LUT flagging range (Figure 7).

The DGA LUT flagging ranges derived as the outer limits of all analyzed orbits (Table 1) are listed in Table 3.

4.3.1 Vs. official On-orbit LUT

The official VIIRS SDR DGA LUT was updated using selected earth scenes collected between November 23, 2011 and December 21, 2011 [6]. The subsequent analysis show no LUT update needed as the DGA drift is very small and likely within the uncertainty of anomaly boundary determination.

In Figure 9, the vertical bars in the top plot shows the detector dependent DGA flagging ranges listed in Table 3. The DGA flagging ranges shows small detector variation within each band. The middle plot in Figure 9 shows the differences between the DGA ranges listed in Table 3 and the updated official on-orbit LUT values. The plot shows the DGA upper limits (blue starts) determined in this analysis are similar (~ 5 DN variation). The lower limits (blue stars) are 10 to 20 DN higher than the LUT. The slightly smaller DGA ranges (~10 – 15 DN) could come from the different algorithms used in determining the anomaly boundary in the histogram. As the DGA limit is determined is less conservatively at its lower bound (see Section 3), the slightly higher lower bounds could be expected.

4.3.2 Vs. Pre-launch

The bottom plot in Figure 9 shows the differences between DGA ranges listed in Table 3 and the pre-launch derived values [4, 5]. The DGA LUT is compared with the RC-2 test configuration (auto gain, nominal temperature plateau, electronic side B), that is closest to the on-orbit condition. The plot shows the DGA upper limits (blue stars) determined in this analysis are about 15 to 40 DN higher than the pre-launch values. The lower limits (red cross) are about 10 to 40 DN lower. The DGA range differences could result from the different methods (DN ramp vs. histogram) as well as the variation in instrument conditions during data collection. The pre-launch DGA ranges were defined using DN ramps in multiple power steps to ensure accurate determination. In addition, the pre-launch data is collected within a much shorter time period in a thermal chamber [4, 5] than the 8 months data collection period in this analysis. Compared with on-orbit operation, the test environment should have more stable DCR, dark offset and instrument condition. The more precise pre-launch method and stable test environment likely result in tighter anomaly region.

5. Conclusion

The on-orbit VIIRS Dual Gain Anomaly (DGA) phenomenon on Suomi NPP was observed and cross examined with MODIS Simultaneous Nadir Overpasses (SNOs). The anomaly affected region was determined using Earth scene data during the first 8 month period after VIIRS opened its nadir door. The DGA characteristics was tracked weekly and compared with the official DGA flagging LUT and prelaunch analysis.

The analysis showed the DGA can be determined per orbit as the Earth scene radiance distribution of a complete orbit provides a sufficient number of samples with ideal radiance distribution near the anomaly region for identifying the anomaly boundaries. The determined orbital DGA boundaries show the anomaly region normally covers 70 – 80 DN and can shift up/down by roughly 20 DN temporally. The DGA temporal shift is mostly caused by the DCR offset change as the anomaly is affected by both detector and DCR inputs to the electronic. As

the VIIRS DCR algorithm is designed to maintain the detector offset within a small range, the accompanied DGA variation is expected.

The estimated DGA flagging range based on the outer limits of all analyzed orbits' upper and lower boundaries is about 90 – 100 DN, which is about 2.5 % of high gain dynamic range. These DGA ranges compare well with the currently implemented on-orbit LUT, with LUT slightly over flagging about 20 DN at the lower limits. Prelaunch DGA ranges were noticeably smaller due to more stable DCR from the shorter data collection time. The prelaunch DGA ranges were 30 – 50 DN smaller and are within the DGA range determined in this analysis.

Finally, the challenge remains on assessing the impact of VIIRS dual gain anomaly on long-term Environmental Data Records (EDRs) and global Earth sciences and how to minimize the anomaly impact by better characterization and anomaly correction in the future calibration efforts.

References:

[1] W. L. Barnes, T. S. Pagano, and V. V. Salomonson, “Prelaunch characteristics of the Moderate Resolution Imaging Spectroradiometrer (MODIS) on EOS-AM1”, IEEE Trans. Geosci. Remote Sensing, V. 36, no. 4, p1088 – 1100, July, 1998.
[2] Steve Mills and L. Liao, “Dual gain anomaly (DGA) quality flag algorithm issues & on-orbit tracking”, Northrop Grumman report, April 28, 2010.
[3] Steve Mills, “VIIRS SDR Performance Report”, Northrop Grumman D45684, rev. B, July 21, 2010
[4] Shihyan Lee and J. McIntire, “Dual Gain Anomaly (DGA) on VIIRS F1: Preliminary Results”, NICST_REPORT_10_017, September 14, 2010.
[5] Shihyan Lees and J. McIntire “: Characterizing VIIRS F1 Dual Gain Anomaly from RC-2 Measurements”, NICST_MEMO_10_028, November 9, 2010.
[6] Frank Sun, S. Mills, L. Liao, S. Lou, “Test VIIRS Dual Gain Anomaly Tracking ASF with Early NPP Data”, ND_3474907, Northrop Grumman, January 5, 2012.
[7] Junquang Sun and N. Che, “Summary of F1 Radiometric Calibration Performance for RSB from TV RC-02 tests”, NICST_MEMO_10_010, May 3, 2010.
[8] Shihyan Lee, “RAD-25: VIIRS F1 Dual Gain Anomaly Flagging Verification: Preliminary Results”, VCST_TECH_REPORT_11_004, Nov 29, 2011.
[9] Shihyan Lee, “RAD-25: VIIRS F1 Dual Gain Anomaly Flagging Verification: LUT updates ”, VCST_TECH_REPORT_12_002, Jan 17, 2012.
[10] “VIIRS Radiometric Calibration Algorithm Theoretical Basis Document ATBD (ref Y3261), Rev. F”, D43777, Northrop Grumman, June 31, 2010.
[11] Chengbo Sun, A. Wu, K. Chiang, “Further improvement made in VIIRS Telemetry trending tool development”, VCST_TECH_MEMO_12_001, Jun 15, 2012.

Table 1. Dataset used in this analysis.

orbit	year	mon	day
360	2011	11	22
389	2011	11	24
440	2011	11	28
500	2011	12	2
530	2011	12	4
600	2011	12	9
680	2011	12	15
770	2011	12	21
880	2011	12	29
950	2012	1	3
1000	2012	1	6
1020	2012	1	8
1100	2012	1	13
1201	2012	1	21
1301	2012	1	28
1400	2012	2	4
1500	2012	2	11
1599	2012	2	18
1700	2012	2	25
1800	2012	3	3
1904	2012	3	10
2000	2012	3	17
2099	2012	3	24
2200	2012	3	31
2300	2012	4	7
2400	2012	4	14
2500	2012	4	21
2600	2012	4	28
2700	2012	5	5
2800	2012	5	12
2900	2012	5	19
3000	2012	5	26
3100	2012	6	2
3200	2012	6	9
3301	2012	6	17
3400	2012	6	24
3500	2012	7	1

Table 2. Major VIIRS Events Since Launch

Event #	Description	Start-End DOY	Start Date_Time	End Date_
1	NPP Launch	301-301	10/28/2011_09:48z	10/28/201
2	VIIRS Turned On	312-312	11/08/2011_05:44z	11/08/201
3	VIIRS Door Open	325-325	11/21/2011_16:03z	11/21/201
4	VIIRS 1394 Anomaly	329-330	11/25/2011_16:36z	11/26/201
5	Svalbard communication Loss (Cable cut)	331-336	11/28/2011_11:00z	12/02/201
5	RTA stowed for 3 days Sensor Test 1 (ST-1)	343-346	12/09/2011_22:47z	12/12/201
6	RTA rotating at night only, Sensor Test 2 (ST-2)	349-353	12/15/2011_16:32z	12/19/201
7	RTA Stowed for one week Sensor Test 3 (ST-3)	355-362	12/21/2011_17:14z	12/28/201
8	RTA Stowed for 4 days Sensor Test 4 (ST-4)	363-002	12/29/2011_14:36z	01/02/201
9	VIIRS Roll Maneuver (First Lunar View)	004-004	01-04-2012_08:48z	01-04-201
10	VIIRS Cryo-Cooler Door open	018-018	01/18/2012_15:33z	01/18/201
11	VIIRS SDSM Operated once-per-day	019-024	01/19/12	01/24/12
12	VIIRS Roll Maneuver (Roll during two orbits)	034-034	02/03/12	02/03/12
13	VIIRS OBC Warm-Up Cool-Down	037-042	2/6/2012_1400	2/10/2012
14	VIIRS 1394 Anomaly	043-043	02/11/12	02/11/12
15	NPP Yaw Maneuver	046-047	02/15/12	02/16/12
16	NPP Pitch Maneuver	051-051	2/20/2012_18:15z	2/20/2012
17	NPP Roll Maneuver (With Sector Rotation)	063-063	3/3/2012_23:34z	3/3/2012_
18	VIIRS 1394 Anomaly	070-070	03/10/12	03/10/12
19	VIIRS SC Counter Over Flow Anomaly	084-084	03/24/12	03/24/12
20	VIIRS SBC Lockup Anomaly	088-088	3/28/2012_4:22z	3/28/2012
21	NPP Roll Maneuver (With Sector Rotation)	093-093	4/02/2012_22:59z	4/02/2012
22	NPP Roll Maneuver (With Sector Rotation)	123-123	5/02/2012_10:15z	5/02/2012
23	VIIRS OBC Warm-Up Cool-Down	143-146	5/22/2012_12:34z	5/25/2012
24	NPP Lunar Cal. (No Roll, with Sector	152-152	5/31/2012_14:47z	5/31/2012

	Rotation)			
25	NPP SC Anomaly - SDP trip to Earth Point Mode	173-174	6/21/2012_18:00	6/22/2012

Table 3. Dual Gain Anomaly DN range: derived as the outer bound of all analyzed orbits (see Table 1).

	M1		M2		M3		M4		M5		M7	
	Low	High	Low	High	Low	High	Low	High	Low	High	Low	High
Det: 1	3363	3463	3389	3490	3432	3527	3421	3519	3431	3529	3440	3535
Det: 2	3360	3460	3388	3485	3435	3528	3443	3542	3440	3539	3441	3536
Det: 3	3371	3468	3400	3497	3435	3535	3440	3543	3443	3543	3459	3555
Det: 4	3387	3483	3403	3497	3419	3520	3432	3531	3432	3529	3459	3555
Det: 5	3371	3468	3395	3496	3440	3536	3443	3541	3433	3532	3436	3528
Det: 6	3371	3465	3403	3499	3432	3524	3443	3541	3448	3539	3468	3567
Det: 7	3376	3472	3400	3499	3443	3536	3443	3542	3440	3537	3456	3555
Det: 8	3368	3465	3395	3497	3436	3539	3435	3536	3440	3541	3467	3561
Det: 9	3355	3460	3389	3491	3427	3523	3432	3526	3427	3522	3461	3558
Det: 10	3384	3483	3387	3483	3421	3523	3440	3535	3433	3529	3462	3556
Det: 11	3372	3474	3399	3497	3417	3514	3427	3527	3420	3523	3432	3530
Det: 12	3355	3455	3379	3475	3411	3508	3432	3528	3427	3524	3440	3535
Det: 13	3368	3464	3384	3482	3419	3520	3427	3523	3411	3511	3427	3522
Det: 14	3368	3458	3379	3476	3432	3526	3421	3522	3432	3529	3440	3539
Det: 15	3371	3467	3388	3489	3411	3507	3433	3535	3427	3523	3452	3548
Det: 16	3379	3472	3397	3495	3421	3523	3432	3529	3440	3536	3459	3552

[delete? Info in Figure 9]

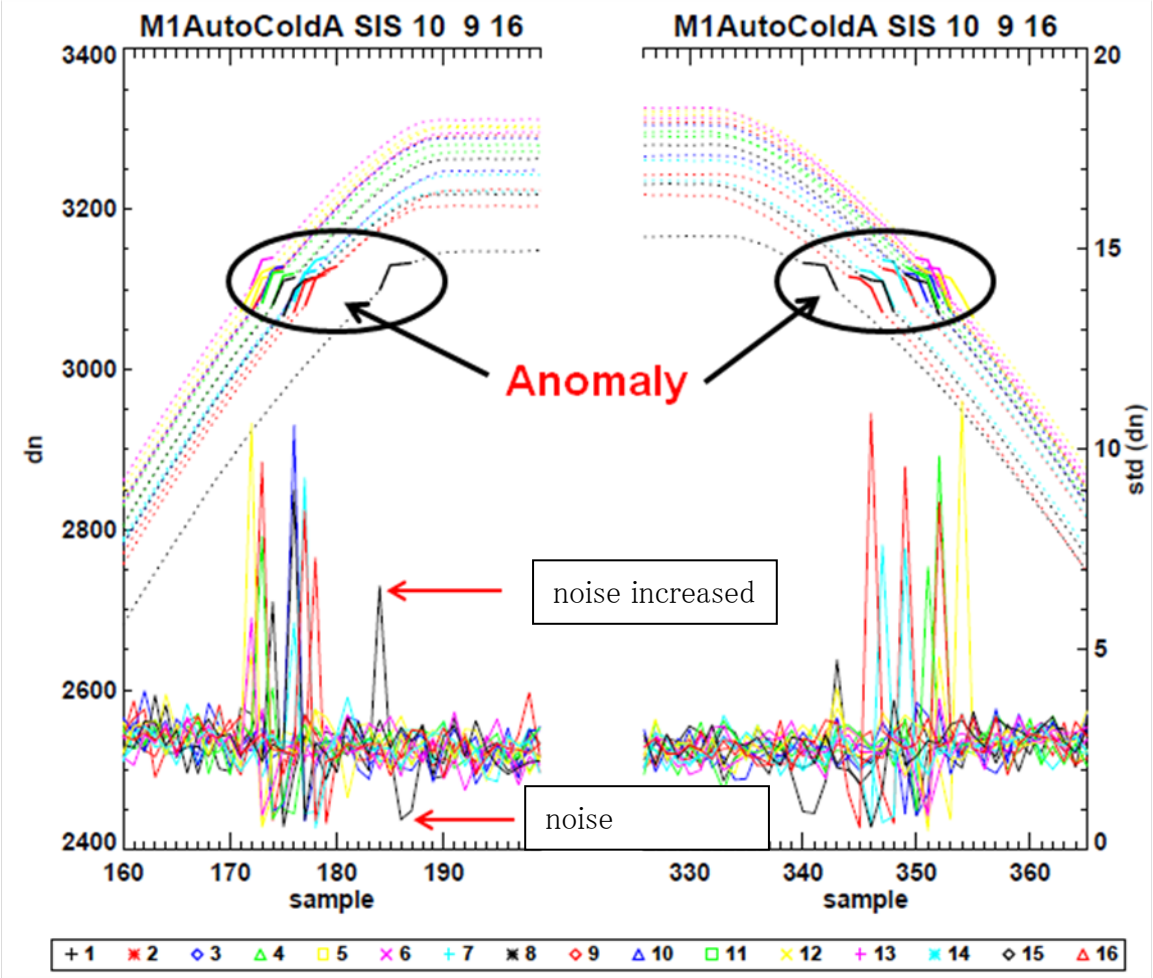

Figure 1. The dotted lines are the measurements in RC-2 for M1 (Auto Gain, Cold plateau, electronic side A) for bulb configuration 10 - 9 - 16 (200 - 45 - 10 W). The plateau shows the location of full SIS-100 aperture view, and to the left/right are the SIS-100 ramps. The solid lines at the bottom show the noise (refer to the right y-axis). Each line represents one detector. The DGA region is marked as solid lines on the ramp.

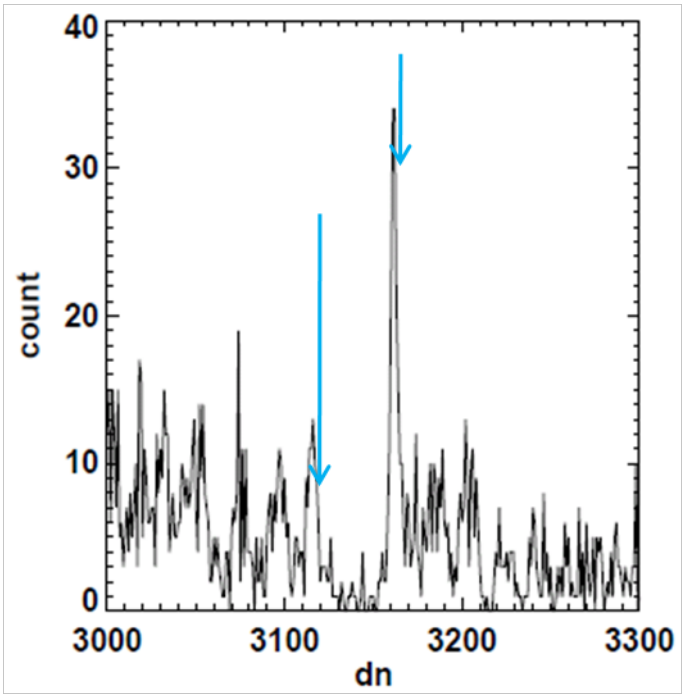

Figure 2. The plot shows the dn histogram for M1 detector 1 (bin size = 1 DN). The region affected by DGA is indicated by blue arrows.

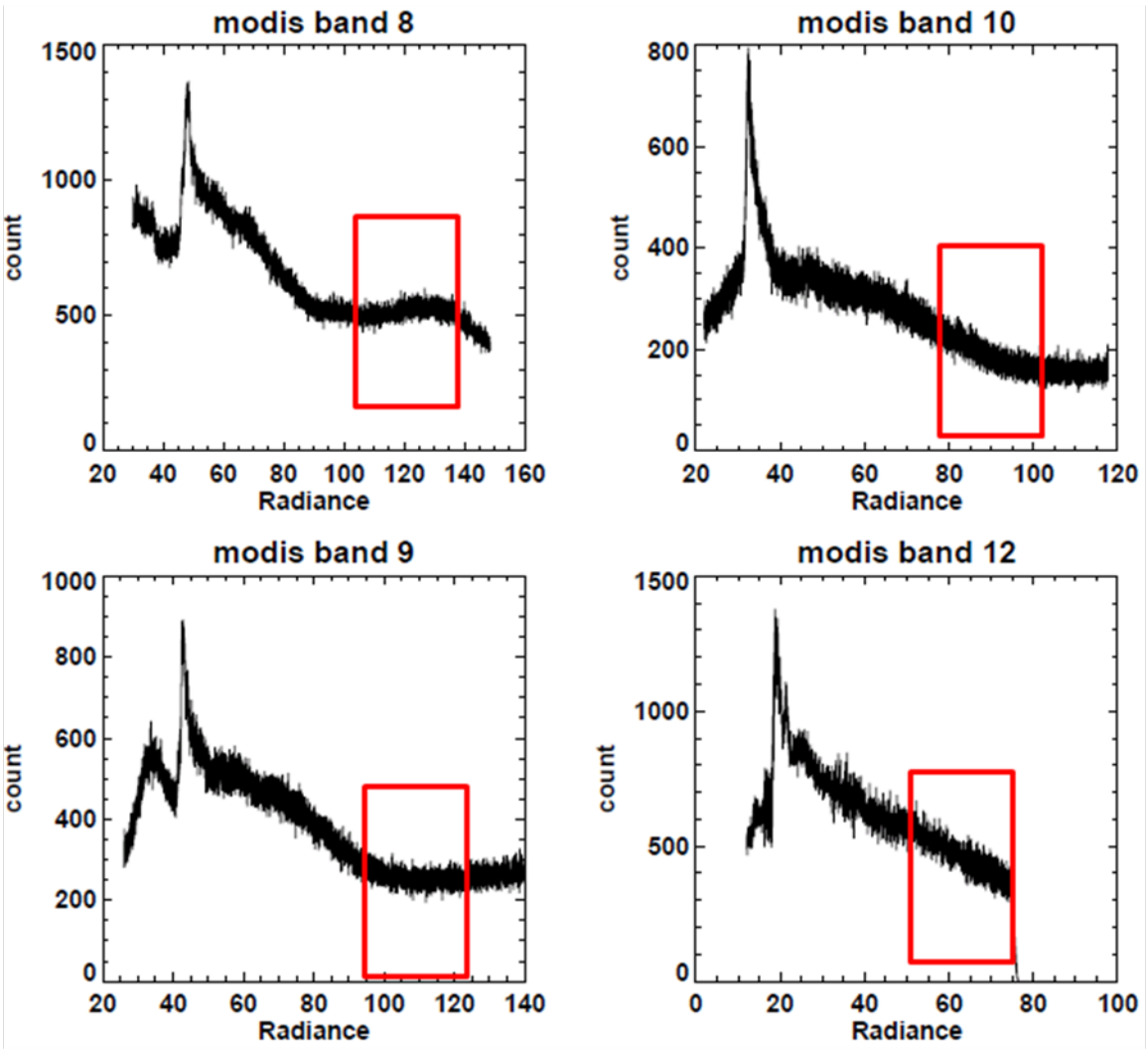

Figure 3. The Radiance histogram generated using Simultaneous Nadir Overpasses (SNOs) MODIS Aqua data, (time period: 2011/11/21 21:30-21:40). Red boxes indicate radiance ranges near corresponding VIIRS DGA. The bandpasses of VIIRS M1 to M4 roughly correspond to MODIS band 8, 9, 10, and 12.

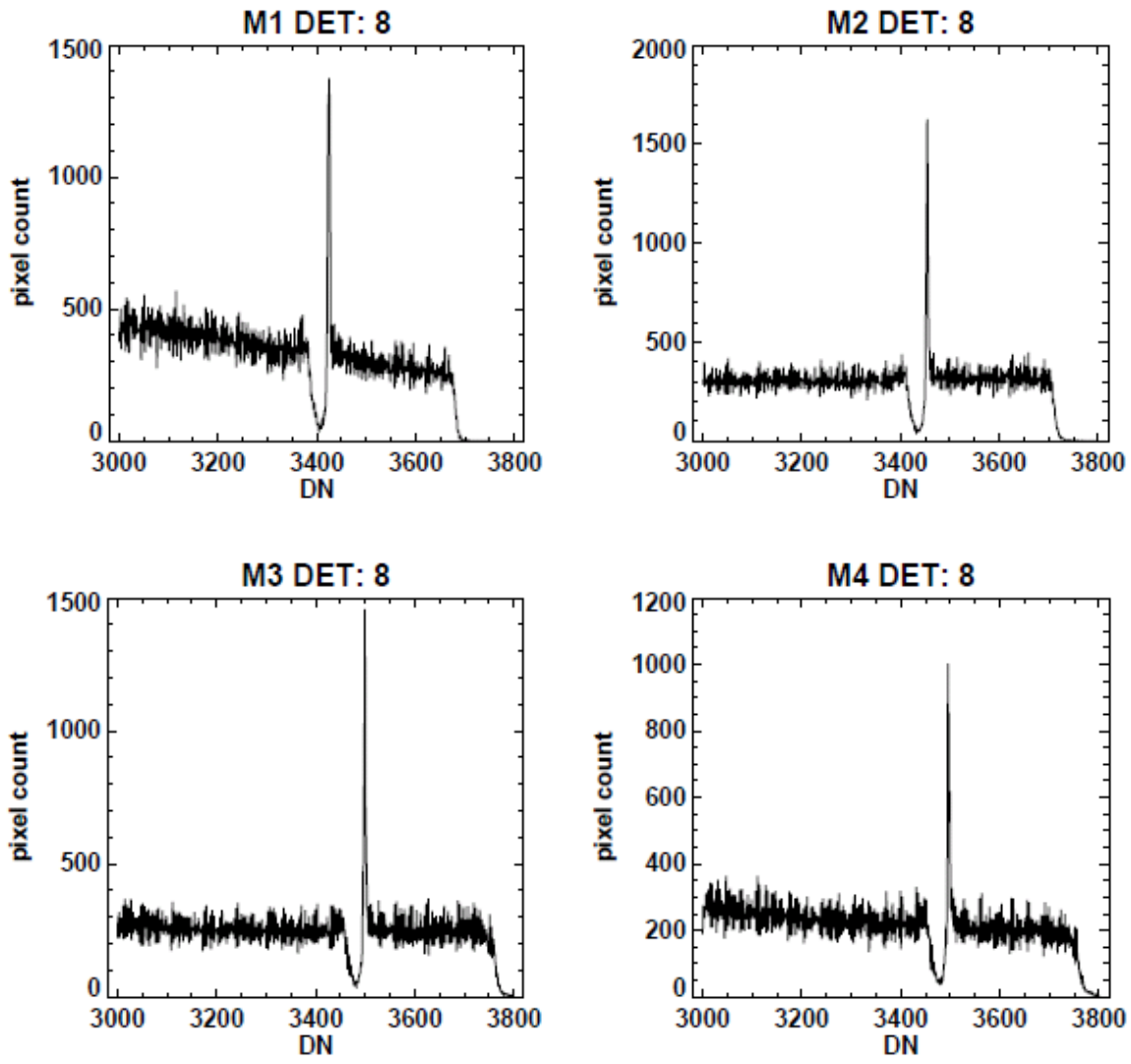

Fig. 4 The DN histogram generated using Simultaneous Nadir Overpasses (SNOs) VIIRS data, (time period: 2011/11/21 21:30-21:40). The bandpasses of VIIRS M1 to M4 roughly correspond to MODIS band 8, 9, 10, and 12..

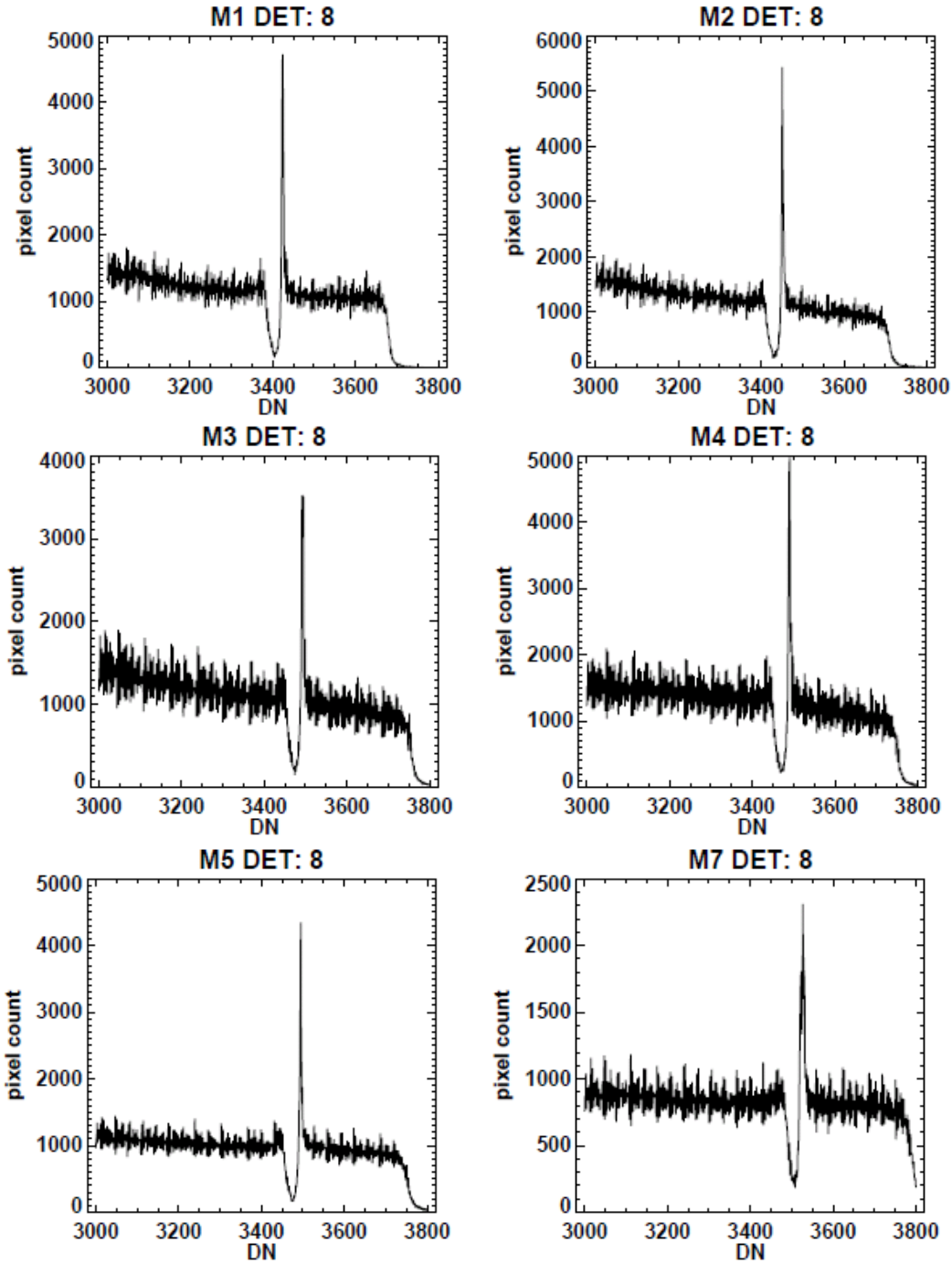

Figure 5 Orbit 3000, dual gain band (high gain) DN histogram (bin size = 1) for middle detector. Note: edge detector (detector 1, 2, 15, 16) will have lower pixel counts due to bow-tie deletion.

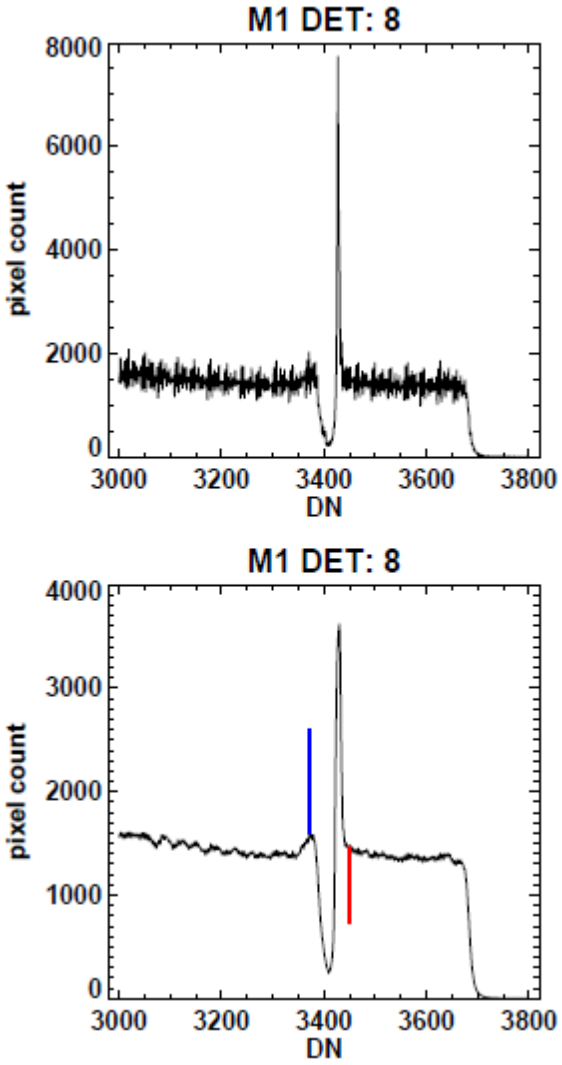

Figure 6: Tracking DGA using a DN histogram. M1 middle detector data collected in orbit 360 were used in this example. Top plot shows the raw DN histogram. Bottom plot show the smoothed histogram used to determine DGA limits. The blue and red vertical lines indicate the anomaly lower and upper bounds.

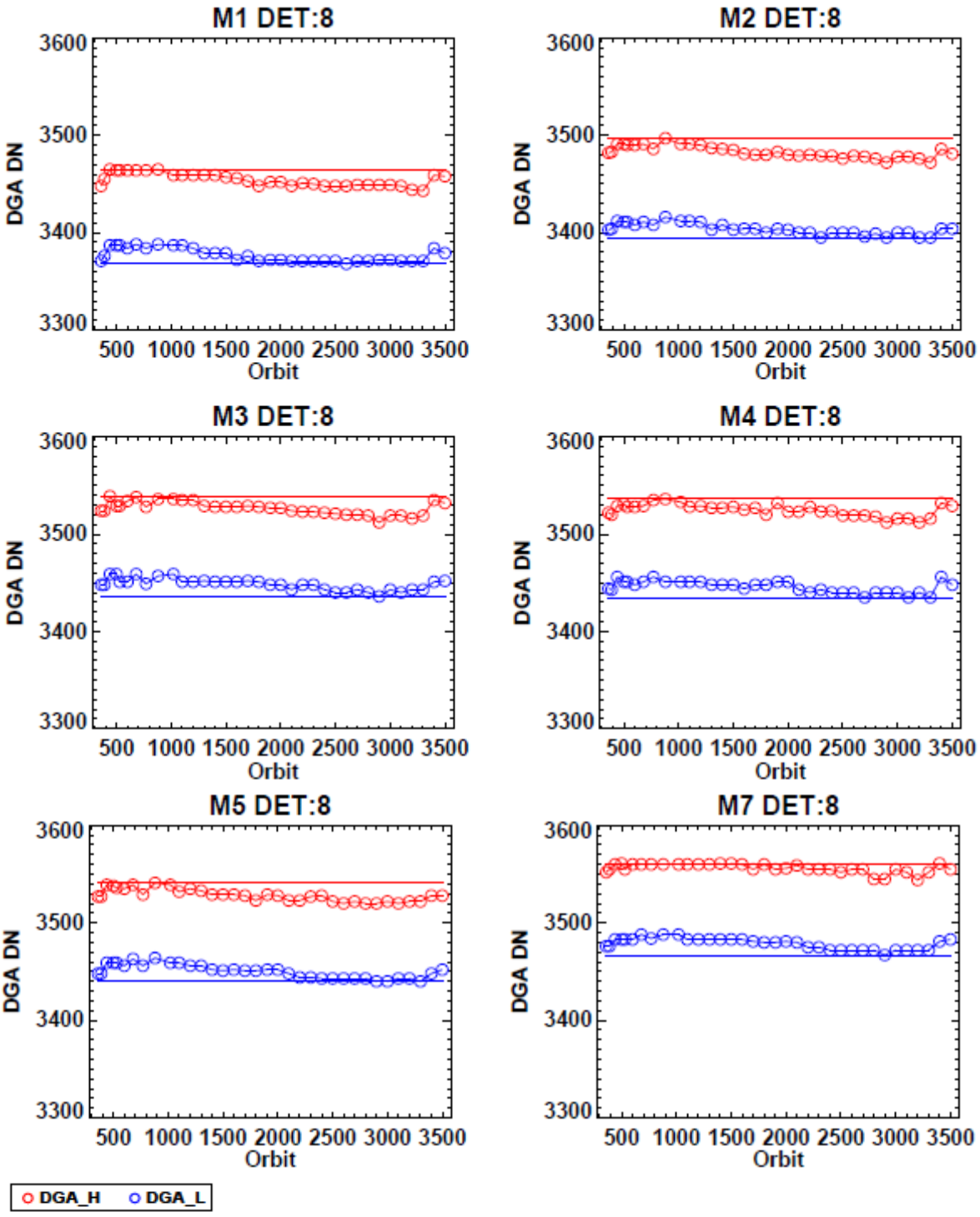

Figure 7. DGA anomaly trending for middle detector (Det: 8). The red/blue circles indicating the anomaly's upper/lower limits for each of the analyzed orbits (see Table 1). The red/blue horizontal lines indicating the maximum and minimum of the upper and lower limits for all analyzed orbits.

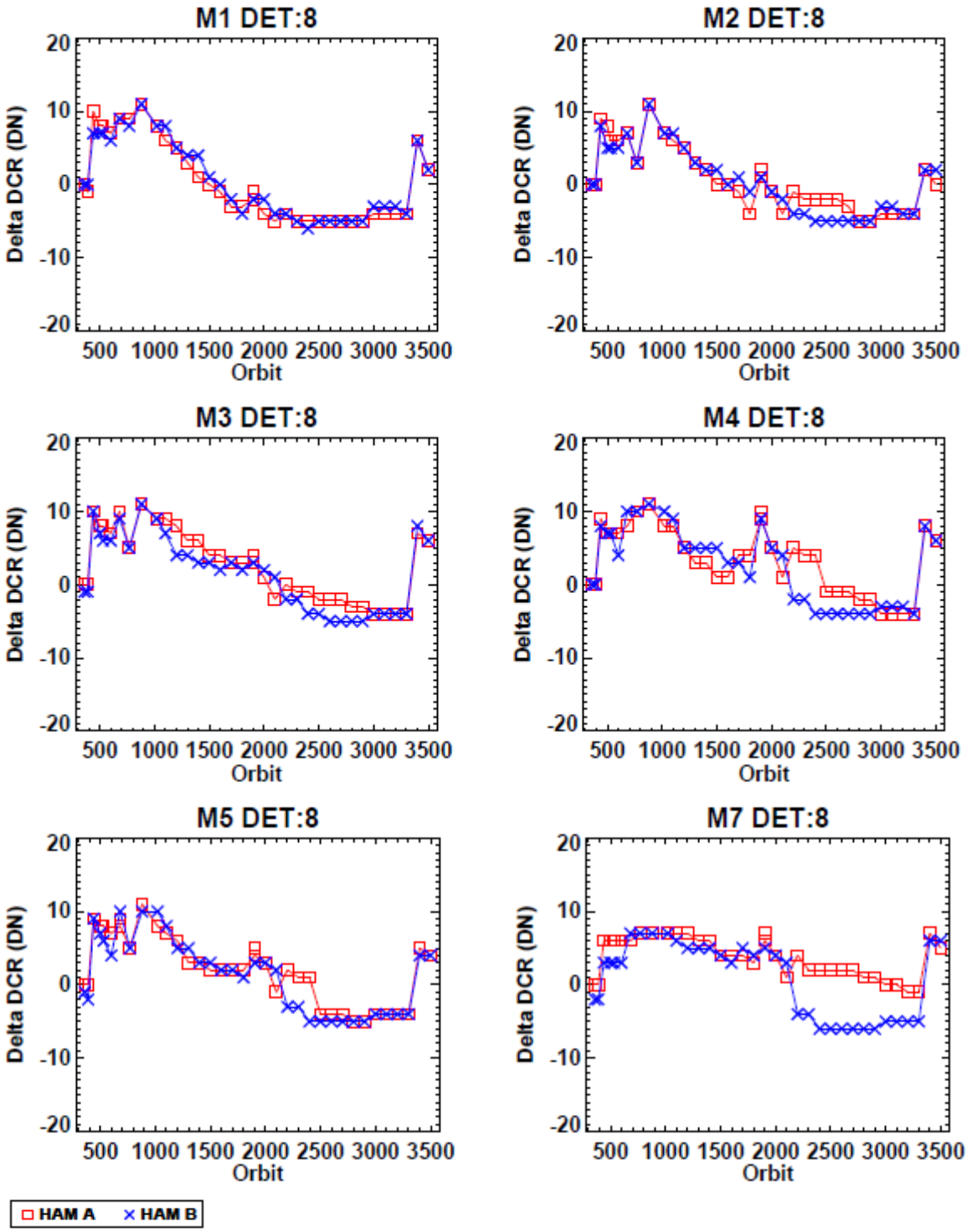

Figure 8. Delta DCR trending. Delta DCR is the DC Restore offset DN difference from the first analyzed orbit (360). The DCR offset is HAM side dependent, and is indicating by red rectangular (HAM A) and blue cross (HAM B).

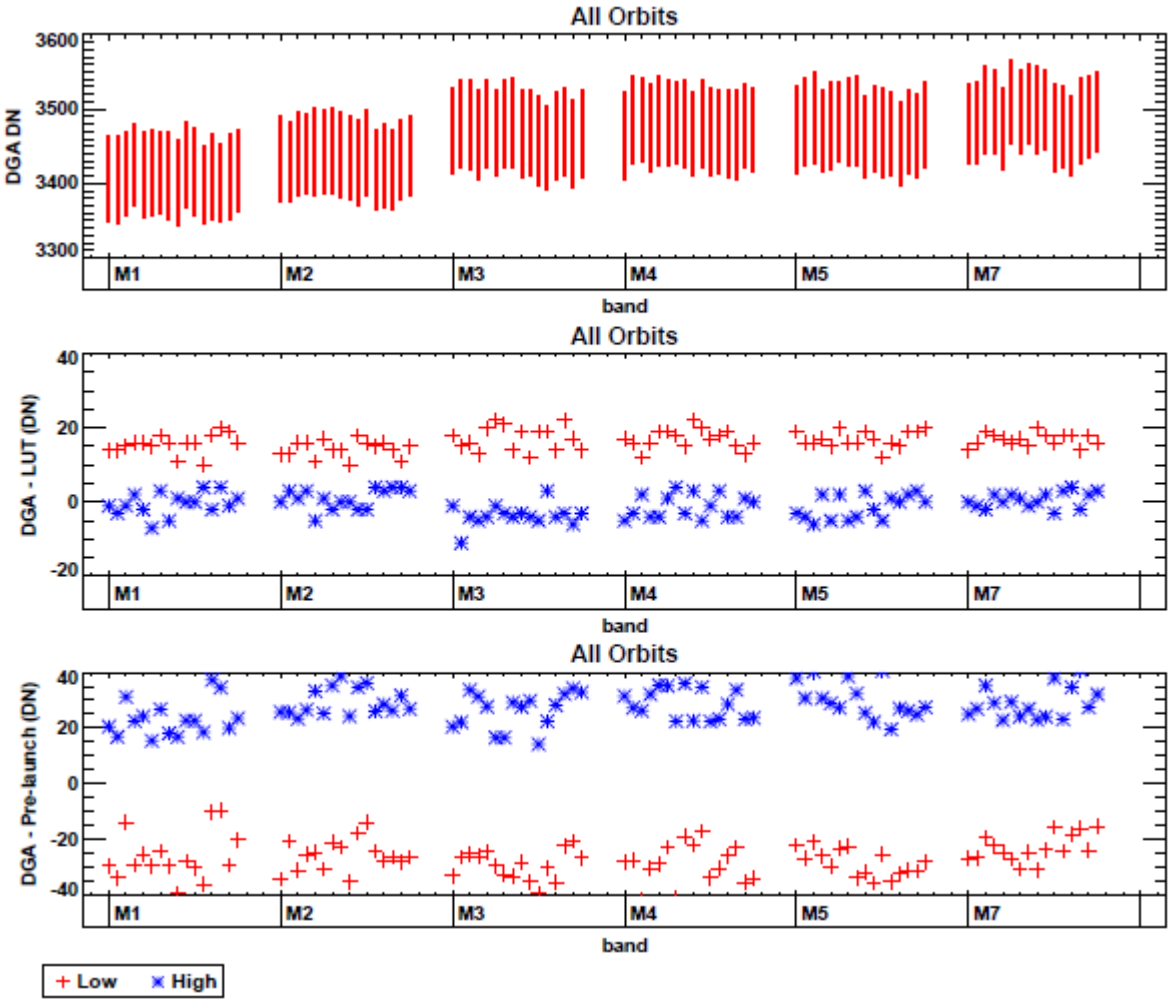

Figure 9. Comparison of the determined DGA flagging range with first official on-board DGA LUT update and pre-launch analysis derived using RC-2 data from nominal temperature plateau. For each band, the 16 detectors are plotted from left-to-right along the x-axis. Top: DGA flagging range determined as the outer limits of all analyzed orbits. Middle: DGA vs. DGA LUT, Red/blue symbols indicate upper/lower limits differences, defined as [DGA] - [DGA_LUT]. Bottom: DGA vs. DGA LUT, Red/blue symbols indicate upper/lower limits differences, defined as [DGA] - [DGA_Pre-launch].